Optimization of layered material configuration for shock attenuation

J. Verreault*, M.M. van der Voort

TNO, 137 Lange Kleiweg, Rijswijk, 2280 AA, The Netherlands
*jimmy.verreault@tno.nl

Abstract
Multi-layered materials with alternating impedances as a mean to mitigate sympathetic detonation is considered in this investigation by studying the wave scattering and energy absorption phenomena. This is achieved using an analytical wave-tracking model that accounts for the different wave interactions within and at the interface of each layer. It is shown that there is a critical areal density of the overall multi-layered system beyond which the performance is increased significantly due to a larger amount of energy absorption. This trend is increasingly significant for increasing impedance mismatch between the different layers. It is also shown that increasing the number of interfaces increases slightly the system performance. The analytical results are supported by numerical simulations. Furthermore mitigation of sympathetic detonation using multi-layered materials is demonstrated experimentally.

Keywords: Multi-layered material; sympathetic detonation; wave-tracking model; blast attenuation; wave scattering.

INTRODUCTION

Impact loading and/or blast loading on a structure or a munitions item can lead to disastrous consequences and adequate protection is required to limit them. Commonly considered methods to attenuate such loading are porous materials, such as foams or sand, and multi-layered materials. Foam materials are capable to absorb energy during the crushing phase of its skeleton material. In contrast, multi-layered materials rely on the impedance mismatch between each layer to scatter the shock waves across the system. Most of the studies on shock-loaded multi-layered material systems were applied to laminate composite materials. Lundergan *et al.* [1], Oved *et al.* [2] and Zhuang *et al.* [3] performed flyer impact experiments and measured the stress evolution within the multi-layered system. Different models were developed to describe the shock scattering effect. Barker [4] used a homogeneous approach to describe this effect using a viscous model. Discrete layers were considered by a number of investigators using the same governing equations but different solution methods such as the unit cell method [5], Floquet's theory with periodic coefficients [6] and wave-tracking algorithms [7,8].

The aim of the present analysis is to provide an understanding of the scattering and energy absorption mechanisms in shock-loaded multi-layered material systems using an analytical wave-tracking model. An optimization of the multi-layered configuration is also performed to minimize the transferred shock pressure and to maximize the energy absorption. The analytical results are supported by experimental and numerical results.

To demonstrate a possible application of this analysis the mitigation of sympathetic detonation is considered. In this application a donor explosive is detonated and its casing impacts the multi-layered material system which covers the acceptor explosive. The criterion for determining whether shock initiation occurs in the acceptor explosive depends on both the shock pressure and the energy fluence [9]. The analysis with the analytical wave-tracking model provides both parameters, although no criterion for shock initiation is chosen, since it depends on the specific explosive. Nevertheless the performance of a

given multi-layered configuration can be assessed based on these parameters. Note that this study is also relevant for other applications, such as shock-loaded laminate composite materials [6] or shock-loaded coated metals under water [10].

MODEL DESCRIPTION

Planar one-dimensional waves are considered across which the Rankine-Hugoniot relations are applied to ensure conservation of mass, momentum and energy:

$$\begin{aligned} \rho u &= \rho_o u_o \\ p + \rho u^2 &= p_o + \rho_o u_o^2 \\ \frac{p}{\rho} + e + \frac{u^2}{2} &= \frac{p_o}{\rho_o} + e_o + \frac{u_o^2}{2} \end{aligned} \tag{1}$$

where ρ is the density, u is the velocity, p is the pressure and e is the internal energy. In addition the particle velocity / shock velocity linear relation is expressed as:

$$U = c_o + su \tag{2}$$

where U is the shock velocity and c_o and s are empirically determined constants for each material. The Hugoniot equation is obtained by re-arranging the set of Eq. (1):

$$e - e_o = \frac{1}{2}(p + p_o)(v_o - v) \tag{3}$$

where $v = 1/\rho$. The Hugoniot equation represents the locus of all possible shocked states and is shown in Fig. 1. For this example the initial pressure p_o is arbitrarily chosen as 0. Considering the shocked state 1, the increase of internal energy from state 0, according to Eq. (3), is the total area under the so-called Raleigh line. The unloading process however follows the isentrope which is different but close to the Hugoniot. Approximating the isentrope by the Hugoniot, the decrease in internal energy across the rarefaction wave is given by:

$$e_1 - e_o = \int p dv \qquad \text{(along the Hugoniot)} \tag{4}$$

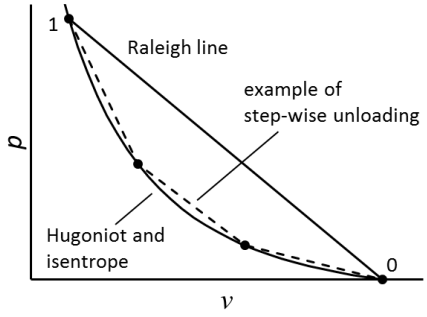

Figure 1. Hugoniot curve and Raleigh line in the $\boldsymbol{p - v}$ plane.

There is therefore a net increase of internal energy (area between the Raleigh line and the Hugoniot) as a result of a shock loading / unloading process manifested in reality by an increase of thermal energy. In a shock-loaded multi-layered material system, two phenomena take place: wave scattering and energy absorption (or dissipation). Wave scattering occurs at interfaces between two materials of different impedance, where incident shocks scatter into transmitted and reflected shocks, whereas energy

absorption is the net increase of internal energy resulting from the loading / unloading processes. To calculate the overall energy absorption all wave interactions (hence all loaded and unloaded states) must be taken into account. The treatment of the different types of wave interaction can be found in shock wave textbooks [9].

In the analytical wave-tracking model used in the present analysis a number of assumptions are made. First, the material response is assumed to be in the shock regime and the deformation is purely hydrodynamic. Second, rarefactions are considered as discontinuities with a single propagation speed. For the case of a single loading / unloading process from and to a given initial state, this assumption would generate a significant discrepancy compared to using the Hugoniot curve for the unloading step. However for a step-wise unloading process (such is the case in shock-loaded multi-layered materials) the discrepancy is not as significant, as shown in Fig. 1 with the dashed lines. Third the spall phenomenon is not considered in this analysis, although two layers are free to separate from each other. Fourth, a wave is discarded whenever the pressure difference across the wave is lower than 1%.

MODEL VALIDATION

The experimental investigation of Zhuang *et al.* [3] is used to validate the wave-tracking model. The experimental setup is schematically shown in Fig. 2. A flyer plate impacts a multi-layered system of low- and high-impedance materials. A stress gauge (manganin gauge) is used at a specified distance from the impact surface. The material properties are provided in Table 1. The flyer plate is made of polycarbonate (PC) or aluminum (Al). The low-impedance material is PC whereas the high-impedance materials are stainless steel (SS) or glass (GS).

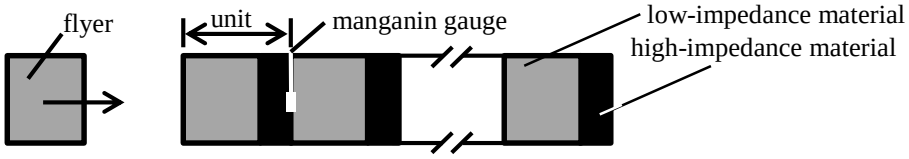

Figure 2. Schematic of the experimental setup used by Zhuang *et al.* [3].

Table 1. Material properties used for the simulations of the experimental tests of Zhuang *et al.* [3].

Part	Material	Thickness (mm)	Density (g/cm^3)	c (m/s)	s
Flyer	PC	2.87	1.19	2.40	1.526
Flyer	Al	5.55	2.79	5.33	1.338
Low-impedance material	PC	0.74	1.19	2.40	1.526
High-impedance material	SS	0.37	7.89	4.60	1.47
High-impedance material	GS	0.55	2.50	5.20	0.0

Five cases are considered for the validation of the wave-tracking model. The test conditions for these five cases are given in Table 2. In this table, the material identification also includes the thickness in hundredths of a millimeter (for instance PC74 refers to a polycarbonate plate with a thickness of 0.74 mm). The pressure profiles are presented in Fig. 3. Referring to Case 1, the analytical profile follows reasonable well the experimental results until the pressure is release at 1.7 μs. A good qualitative agreement is also observed for Case 2 although quantitatively the pressure level is slightly larger from the wave-tracking model. In Case 3, both the analytical and experimental results exhibit three consecutive peaks, although they are slightly broader and lower from the wave-tracking model. A reasonably good agreement is reached for both Cases 4 and 5 before the pressure is released at 3 μs and 3.3 μs, respectively. Globally, most of the features are reproduced by the wave-tracking model especially before the pressure release starts to occur.

Table 2. Test conditions from the experimental investigation of Zhuang *et al.* [3].

	Flyer material	Impact velocity (m/s)	Materials and thickness (mm)	Number of units	Location of the manganin gauge from the impact surface (mm)
Case 1	PC287	1062	PC74 / SS37	8	0.74
Case 2	PC287	561	PC74 / SS37	8	0.74
Case 3	Al555	1070	PC74 / GS55	7	3.32
Case 4	PC287	1056	PC74 / GS55	7	3.32
Case 5	PC287	563	PC74 / GS55	7	3.32

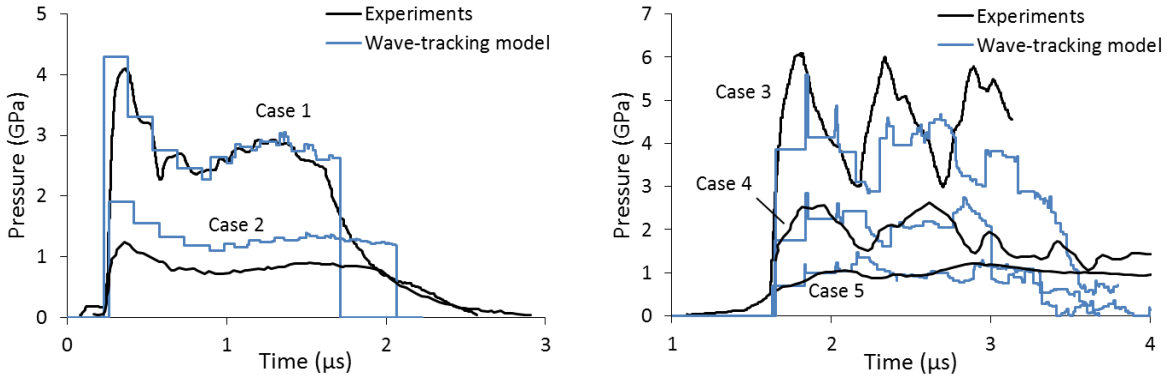

Figure 3. Comparison of the pressure profiles from the wave-tracking model and the experiments of Zhuang *et al.* [3]. The different cases are defined in Table 2.

OPTIMIZATION

Configuration

The purpose of the optimization study is to explore the influence of the different parameters of the multi-layered system on its performance (its ability to attenuate the shock wave and the energy fluence in the acceptor explosive). A schematic of the considered configuration is presented in Figure 4. The casing of the donor is assumed to be a flyer plate with a velocity of 1500 m/s. The flyer impacts a system of low- and high-impedance materials. The casing and explosive of the acceptor are located behind the multi-layered system and the acceptor explosive is assumed to be semi-infinite. The materials used for the optimization study are listed in Table 3. The flyer and casing are made of stainless steel whereas the high-impedance materials are Magnesium (Mg), aluminum (Al) and ceramic (Cer). The low-impedance materials are rubber (Rub), polyethylene (PE) and Nylon (Ny), whereas the acceptor explosive is Semtex. For each material the density, acoustic impedance (Z) and parameters of the shock velocity / particle velocity relationship Eq. (2) are provided.

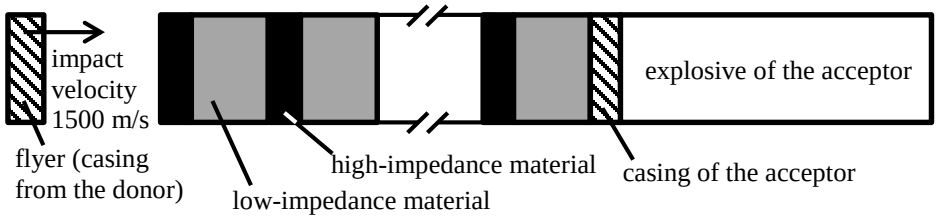

Figure 4. Schematic of the configuration used for the optimization study of multi-layered materials.

Table 3. Material properties used in the optimization study of multi-layered materials.

Part	Material	Density (g/cm^3)	c (km/s)	s	Z (MPa*s/m)
Flyer and casing	SS	7.90	4.57	1.49	36.1
High-impedance material	Mg	1.74	4.49	1.26	7.81
High-impedance material	Al	2.79	5.33	1.34	14.8
High-impedance material	Cer	3.83	7.0	1.30	26.8
Low-impedance material	Rub	1.01	0.85	1.87	0.86
Low-impedance material	PE	0.92	2.90	1.48	2.65
Low-impedance material	Ny	1.14	2.57	1.85	2.93
Acceptor explosive	Semtex	1.60	1.33	1.99	2.13

Baseline case

As a baseline configuration a Cer/Rub single unit is considered with the thickness of the ceramic layer (6.3 mm) equal to half that of the rubber layer (12.6 mm). The wave diagram for this case is displayed on the left-hand side of Fig. 5 showing the propagation of compression waves (blue lines), rarefaction waves (red lines) and interfaces (dashed lines) in time. The flyer is initially located within the layer A. The ceramic and rubber layers correspond to layers B and C, respectively. The acceptor is indicated by the layers D (casing) and E (explosive). The interaction between the different waves and at the interfaces can be observed as well as the motion of the different layers in time. The evolution of the total energy (kinetic and internal energies) in the different layers is presented in the center graph of Fig. 5. The energy in the flyer quickly decreases from its initial value of 40 MJ/m^2 to 5.4 MJ/m^2 (part of which 1.1 MJ/m^2 is kinetic). There is therefore 34.6 MJ/m^2 transferred to the multi-layered system and the acceptor. The energy in the ceramic quickly increases to 28 MJ/m^2, but also decreases back to zero after 15 µs. However the final energy in the rubber does not drop below 20.4 MJ/m^2, which is the amount of internal energy that is effectively absorbed. The parameter of interest for sympathetic detonation is the energy fluence in the explosive of the acceptor defined as:

$$E_{fluence} = \int pudt \tag{5}$$

where p and u are taken at the casing / explosive interface. As shown in Fig. 5 the energy fluence at the casing / explosive interface is significantly lower than the case of a non-protected acceptor. From the pressure profile on the right-hand side graph the maximum pressure recorded at the casing / explosive interface is 2.6 GPa.

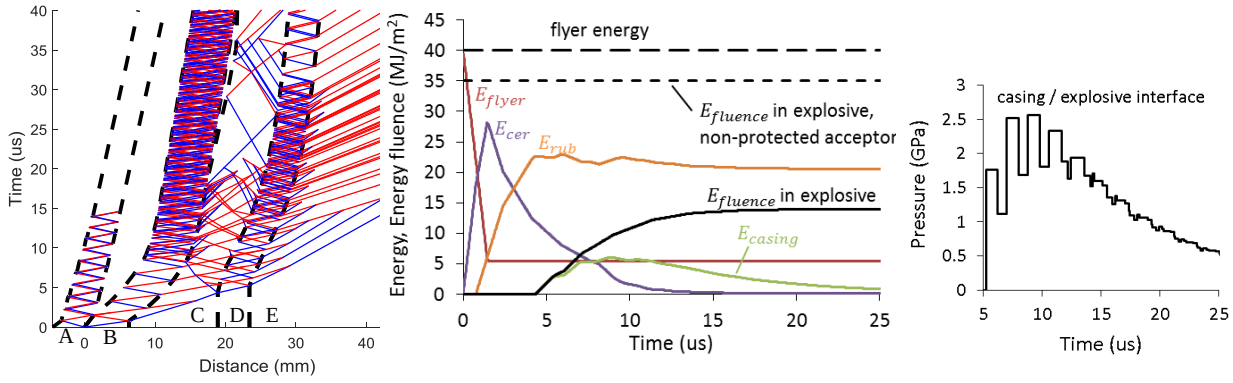

Figure 5. Wave diagram, energy in the different layers and pressure profile at the casing / explosive interface for a single unit Cer / Rub system with an areal density of 3.7 g/cm^2.

Effect of the areal density

The effect of the areal density is assessed by considering Cer/Rub systems of different thicknesses. The resulting maximum pressure and energy fluence at the acceptor casing / explosive interface is provided in Fig. 6. The diamond symbols refer to the simulations where the thickness of the ceramic layer is half that of the rubber layer, whereas the simulations with a constant ceramic thickness of 7.5 mm (the motivation for this choice is provided below) are indicated by triangle symbols. Referring to the diamond symbols, there is a drastic change of trend at an areal density of 3.7 g/cm^2 for both the maximum pressure and the energy fluence. For lower values the energy fluence varies between 10 and 15 MJ/m^2, whereas the energy fluence decreases to 0.6 MJ/m^2 for areal densities larger than 5 g/cm^2.

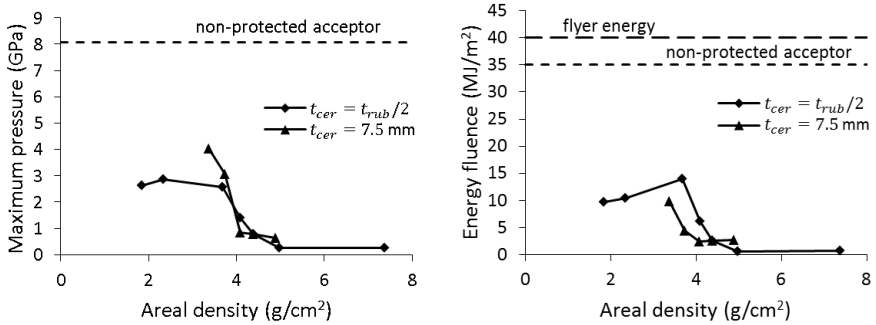

Figure 6. Maximum pressure and energy fluence at the acceptor casing / explosive interface for single unit Cer / Rub systems for different areal densities.

To explain the drastic drop in energy fluence for areal densities larger than 3.7 g/cm^2, wave diagrams corresponding to areal densities of 3.7 g/cm^2 and 4.4 g/cm^2 at early times after impact are presented on the left-hand side of Fig. 7. For the case of an areal density of 3.7 g/cm^2, the rarefaction labelled R1 in the flyer reached the flyer / ceramic interface at approximately 1.3 μs. The rarefaction R2 in the ceramic reaches the same interface shortly before the flyer rarefaction R1. However, for an areal density of 4.4 g/cm^2, it is the flyer rarefaction R1 that arrives at the flyer / ceramic interface first. Because of this difference there is a double-wave pattern in the ceramic layer of the 4.4 g/cm^2 case and a single-wave pattern in the 3.7 g/cm^2 case. The effect of this different wave pattern on the pressure and velocity at the ceramic / rubber interface is displayed on the right-hand side graphs. Referring to the pressure profiles, a step-wise decrease of pressure is observed for the 3.7 g/cm^2 case. However, for the 4.4 g/cm^2 case, every release step is preceded by a substantial unloaded state (down to below 0.4 GPa). In other words, in the 3.7 g/cm^2 case the interface is loaded / unloaded once (between 0 and 8 μs) whereas this is repeated five times in the 4.4 g/cm^2 case. As explained in reference to Fig. 1, the net internal energy increases every time a material is subjected to a load / unload process. Therefore the materials in the 4.4 g/cm^2 case are capable to absorb a larger amount of energy due to the multiple load / unload processes compared to the 3.7 g/cm^2 case.

From the above results it can be concluded that a thickness of 7.5 mm for the ceramic layer is necessary to allow multiple loading / unloading processes at the ceramic / rubber interface and hence increase the energy absorption. The triangle symbols in Fig. 6 refer to different areal densities while keeping the ceramic layer thickness at 7.5 mm. For areal densities lower than 4 g/cm^2 the rubber layer thickness decreases to a level that it can no longer decelerate the ceramic layer efficiently. Therefore the energy fluence increases for areal densities lower than 4 g/cm^2, while no significant gain is observed from the maximum pressure graph.

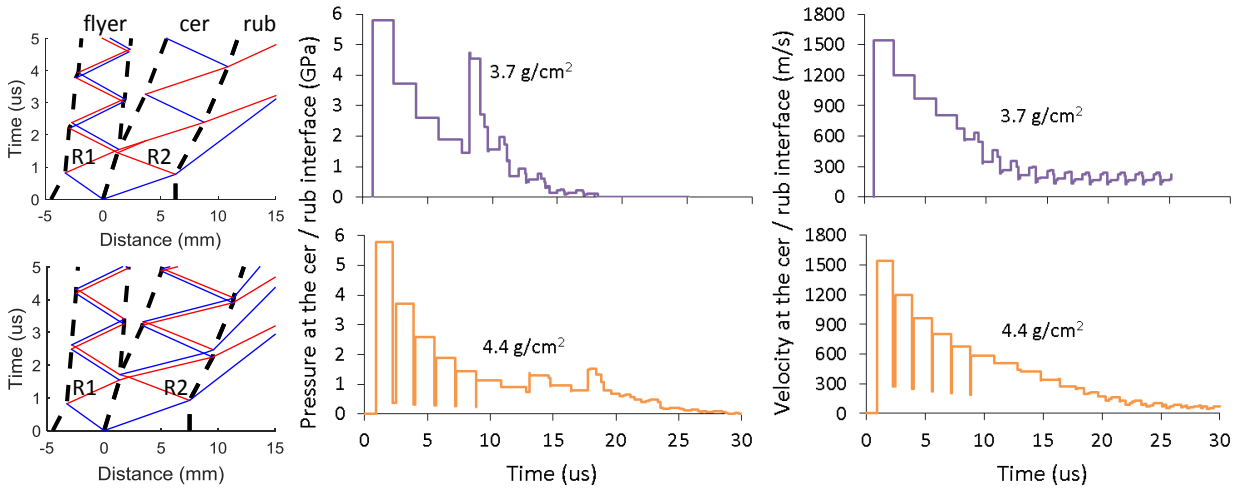

Figure 7. Wave diagram (left), pressure (center) and velocity (right) profiles for a single unit Cer / Rub system with an areal density of 3.7 g/cm^2 (top graphs) and 4.4 g/cm^2 (bottom graphs).

Effect of impedance mismatch and order of material

The impedance mismatch between two materials is given by [6]:

$$I = 1 - \frac{4Z_1Z_2}{(Z_1 + Z_2)^2} \tag{4}$$

where $Z = \rho c$ is the acoustic impedance. The impedance mismatch parameter varies from 0 (no impedance difference) to 1 (infinite impedance mismatch). Three material combinations are considered to study the effect of impedance mismatch: Mg/Ny ($I = 0.21$), Al/PE ($I = 0.485$) and Cer/Rub ($I = 0.88$).

The maximum pressure and energy fluence in the acceptor explosive for the different material combinations is presented in Fig. 8 for different areal densities. The sudden decrease in energy fluence is also observed for the Mg/Ny and Al/PE systems, but at different values of areal densities. Furthermore the higher the impedance mismatch the lower is the energy fluence at areal densities larger than 4 g/cm^2. The effect of the material order is also shown with the PE/Al results. For this case the polyethylene layer is the first to be impacted by the flyer. The sudden decrease of energy fluence does not occur in this case. This is due to the relatively low wave velocity in the polyethylene and therefore the first rarefaction in the flyer always arrives before the first rarefaction in the polyethylene at the flyer/PE interface. In addition, the Al/PE configuration performs significantly better than the PE/Al configuration, especially for areal densities larger than 3.2 g/cm^2.

Effect of number of interfaces

Increasing the number of interfaces inevitably increases the number of wave interactions between the different layers. This is shown on the left-hand side of Fig. 9 with a system of four units of aluminum (labelled B) and polyethylene (labelled C). The resulting maximum pressure and energy fluence at the acceptor casing / explosive interface is shown on the right-hand side graphs with the solid line. For all cases the areal density is kept constant at 4.4 g/cm^2. Increasing the number of units decreases slightly the energy fluence due to the increasing internal energy absorbed in the low-impedance (LI) layers, shown with the dashed line.

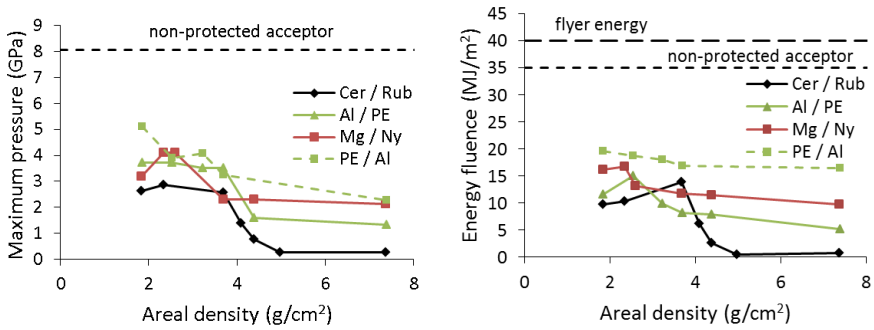

Figure 8. Maximum pressure and energy fluence at the acceptor casing / explosive interface for different material combinations (single unit with $t_{HI} = t_{LI}/2$) and different areal densities.

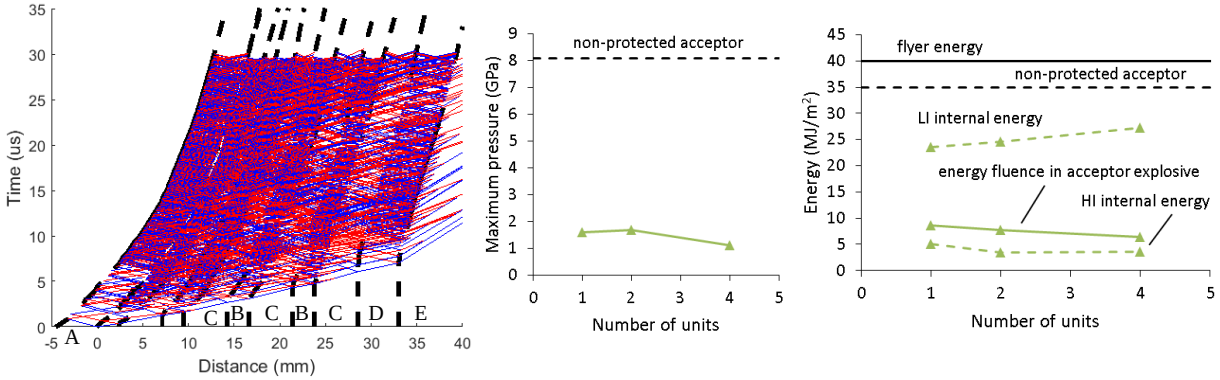

Figure 9. Wave diagram, maximum pressure and energy fluence at the casing / explosive interface for multi-unit Al/PE systems with an areal density of 4.4 g/cm^2 and $t_{HI} = t_{LI}/2$.

COMPARISON WITH EXPERIMENTAL AND NUMERICAL RESULTS

Experiments using layered materials to prevent sympathetic detonation have been conducted at TNO in 2014 [11]. In these experiments cylindrical charge with an inner and outer diameter of 60 and 69 mm, respectively, filled with Semtex 10 were used. Four cases are presented here and the configuration of the multi-layered system for each case is given in Table 4. The distance between the donor and the acceptor is measured from the external face of the casings. The initial setup for Cases 3 and 4 is shown in Fig. 10, as well as the recovered casing for a non-reacted and deflagrated acceptor. The experimental results are also shown on the right-hand side of this figure. A detonation resulted from non-protected acceptors while detonation was prevented for all cases, although a deflagration was observed for the shortest stand-off distances (Cases 3 and 4).

Table 4. Test conditions from the experimental investigation [11].

Case	Multi-layer configuration (■ : Al, ▒ : rub, values in mm)	Overall areal density (g/cm^2)	Distance between donor / acceptor (mm)
1	4 ■ 8 ▒ 4 ■ 8 ▒	4.47	40
2	2 ■ 3 ▒ 2 ■ 5 ▒ 2 ■ 3 ▒ 2 ■ 5 ▒	4.47	40
3	4 ■ 8 ▒ 4 ■ 8 ▒	4.47	24
4	2 ■ 3 ▒ 2 ■ 5 ▒ 2 ■ 3 ▒ 2 ■ 5 ▒	4.47	24

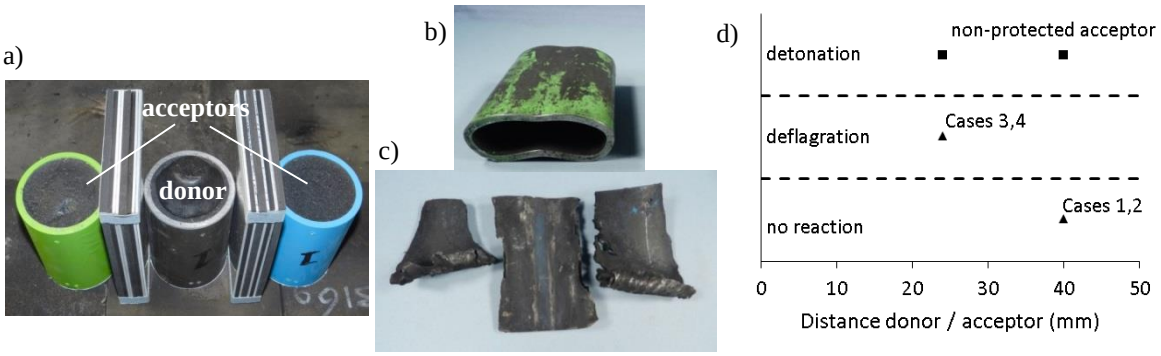

Figure 10. Initial setup for Cases 3 and 4 (a), recovered casing after a non-reacted (b) and deflagrated (c) acceptor and experimental results [11] (d). See Table 1 for the cases definition.

In order to evaluate the accuracy of the wave-tracking model (and to assess the effect of the different assumptions), numerical simulations were conducted using the ANSYS Autodyn V14.0 software. As a qualitative illustration Fig. 11 shows the simulation of Case 1 before initiation of the detonation (left) and shortly after the donor casing impacts the multi-layered system (center). As shown on the right-hand side of this figure the velocity of the donor casing reaches approximately 1400 m/s at the impact which is in close agreement with the velocity calculated with the Gurney equation [12]. The analytical and numerical pressure and energy fluence profiles are compared in Fig. 12. Referring to Case 1 (2 units, 40 mm) the analytical pressure profile follows the trend of the numerical profile, although the numerical values are slightly lower. This is probably due to the lateral expansion waves that are included in the numerical simulation but absent from the analytical calculation (since one-dimensional planar are considered). There is also a good agreement of the energy fluence between the analytical and numerical results. Comparing the numerical profiles for 2 and 4 units (40 mm stand-off), both the maximum pressure and the energy fluence are very similar. The effect of the acceptor standoff distance from the donor can be seen comparing Cases 1 and 3 (2 units 40 mm and 2 units 24 mm). The maximum pressure is slightly lower for the 24 mm case but the shock duration is longer compared to the 40 mm case due to the expanding detonation products. Therefore the energy fluence is larger for the 24 mm case.

The critical maximum pressure and energy fluence for shock initiation of Semtex 10 are not precisely known. However, the critical values for PETN (which is the main constituent at 76% by weight) are in the range of 0.7 – 1.4 GPa [13] and 0.1 – 0.2 MJ/m^2 [14] (at least both thresholds must be exceeded for shock initiation). Referring to Fig. 12 the maximum pressure is near-critical for all cases which explains the experimental observation of no reaction for the 40 mm case and a deflagration for the 24 mm case. This also shows the importance of considering both parameters for the shock initiation criterion.

CONCLUSIONS

A wave-tracking model was used in this study to investigate the wave scattering and energy absorption phenomena in multi-layered material systems for blast and impact loading protection. The analytical model was validated under flyer impact conditions. Varying the areal density of the multi-layered system revealed a critical value beyond which the system performance (based on the transferred shock pressure and energy fluence) is significantly increased due to a larger number of loading / unloading processes in each layer (hence more energy absorbed), especially shortly after impact. The increase in performance beyond the critical areal density was the largest for the material combination with the greatest impedance mismatch (ceramic / rubber). Increasing the number of interfaces for a constant areal density slightly improved the multi-layered system performance. It was shown experimentally that multi-layered materials can help mitigating sympathetic detonation, although a deflagration could not be avoided in the

acceptor for short stand-off distances. It was shown numerically that this is due to a larger energy fluence transferred to the acceptor as opposed to a higher shock pressure.

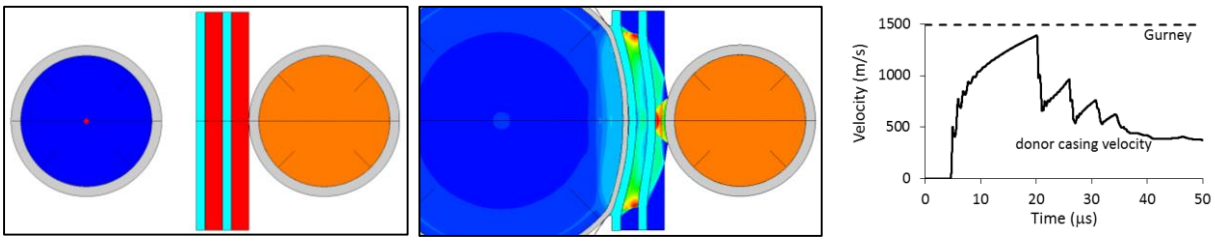

Figure 11. Numerical simulation of Case 1 (see Table 4).

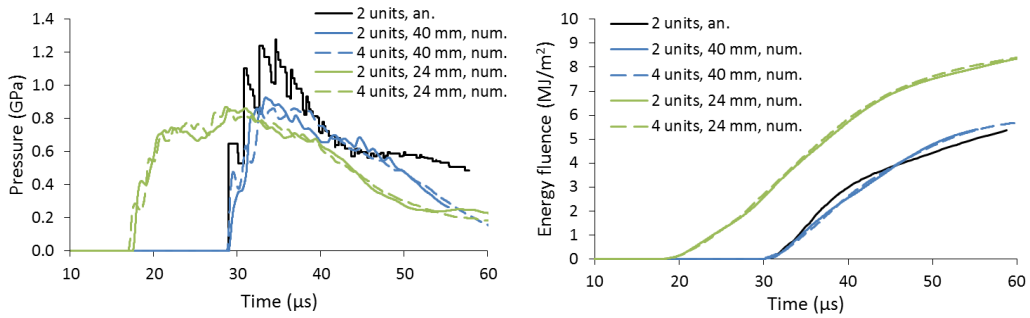

Figure 12. Comparison of the analytical and numerical pressure and energy fluence profiles.

ACKNOWLEDGEMENTS

This investigation was supported by the Dutch Ministry of Defense under the research program V1322 *sustainable ammunition safety*, WP500 *safety of ammunition storage and transport*.

REFERENCES

1. Lundergan, C., and Drumheller, D., *Journal of Applied Physics* 24(2):669-675 (1971).
2. Oved Y., and Luttwak G.E., *Journal of Composite Materials* 12:84-96 (1978).
3. Zhuang S., Ravichandran G., Grady, D.E., *Journal of the Mechanics and Physics of Solids* 51:245-265 (2003).
4. Barker, L.M., *Journal of Composite Materials* 5:140-162 (1971).
5. Clements, B.E., Johnson, J.N., Hixson, R.S., *Physical Review E* 54(6):6876-6888 (1996).
6. Chen, X., and Chandra, N., Composites Science and Technology 64:1477-1493 (2004).
7. Petel, O.E., Jette, F.X., Goroshin, S., Frost, D.L., Ouellet, S., *Shock Waves* 21:215-224 (2011).
8. Agrawal, V., Bhattacharya, K., *International Journal of Solids and Structures* 51:3604-3618 (2014).
9. Cooper, P.W., Explosives Engineering, *Wiley*, 1996.
10. Jin, Z., Yin, C., Chen, Y., Huang, X., Hua, H., *Shock and Vibration* 2014 (2014).
11. van der Voort, M.M., Scholtes, G., Blankers, I.J., Meuken, B., Verreault, J., Hooijmeijer, P., Makkus, J., "Development and cost benefit analysis of mitigating ammunition packaging," TNO 2015 R10113.
12. Gurney, R.W., "The Initial Velocities of Fragments from Bombs, Shells, and Grenades," Army Ballistic Research Lab Aberdeen Proving Ground Report No. BRL-405, 1943.
13. "LLNL Explosives Handbook: Properties of Chemical Explosives and Explosive Simulants," Lawrence Livermore National Laboratory.
14. Keshavarz, M.H., Motamedoshariati, H., Pouretedal, H.R., Tehrani, M.K., Semnani, A., Journal of Hazardous Materials, 145:109-112 (2007).